Astrophysical Masers and their Environments
Proceedings IAU Symposium No. 242, 2007
J.M. Chapman & W.A. Baan, eds.

doi:10.1017/S1743921307012501

Tracing pumping routes in OH

Malcolm D. Gray[1] D. A. Howe[1] and B. M. Lewis[2]

[1]Astrophysics Group, School of Physics & Astronomy, University of Manchester, PO Box 88, Manchester M60 1QD, United Kingdom
email: Malcolm.Gray@manchester.ac.uk

[2]Arecibo Observatory, HC3, Box 53995, Arecibo, PR 00612, U.S.A.

Abstract. We introduce a general method of restoring detailed information about the population flow in molecules under non-local-thermodynamic-equilibrium (NLTE) conditions. This information is usually discarded in numerical algorithms which generate only a solution. We apply the method to tracing the pumping schemes for OH in models that represent three common astrophysical maser environments: the envelopes of asymptotic-giant-branch (AGB) stars, the envelopes of red supergiants, and Galactic star-forming regions. In all three of these cases, we show that a large fraction, typically 0.8 or more, of the maser inversion can be recovered from a set of routes that depend on a much smaller fraction (considerably less than 0.1) of the total number of input coefficients to the model. Therefore, these cases display underlying simplicity in the pumping scheme.

Keywords. masers, molecular data, molecular processes, radiative transfer, methods: numerical, stars: AGB and post-AGB, stars: formation

1. Introduction

Our current knowledge of maser pumping schemes is patchy. In the case of OH, conspicuous successes include the 1612-MHz line in the circumstellar envelopes of AGB and OH/IR stars. This pump was recovered by analytic estimates, backed up by numerical calculations, and was found to be based on the absorption of 35-μm and 53-μm radiation (Elitzur, Goldreich & Scoville (1976); Elitzur (1981); Dickinson (1987)). This absorption is followed by a radiative cascade down the $^2\Pi_{1/2}$ ladder of levels, and then a final cross-ladder transition to the $^2\Pi_{3/2}, J = 3/2$ rotational ground state. A large inversion results if this last transition is optically thick. Observational support for these schemes is so far partial (He & Chen (2004); He *et al.* (2004)), and further observations are required with greater sensitvity and spectral resolution than the LWS instrument aboard the Infrared Satellite Observatory (ISO). A pumping scheme in similar detail for the 1720-MHz line of OH was developed by Elitzur (1976). In contrast to the 1612-MHz scheme, this 1720-MHz pump is driven primarily by collisions with H_2.

By contrast, information about pumping of the OH main-line masers in star-forming regions has been much harder to glean from a variety of observations and models. The models have been employed mainly in parameter-space searches, and these yield only broad inferences from the initial conditions fed into them. For example, a trend that shows increasing maser inversion as a function of dust temperature strongly suggests that far-infrared (FIR) radiation forms part of the pump, but the details are lost because each run of the model, corresponding to a point in the parameter space, provides only an NLTE solution. No details of the population flow are stored. One feature which is expected to be important in main-line pumping is FIR line overlap (for example Bujarrabal *et al.* 1980). Another is a strong continuum FIR field, probably from dust. The combination of this

continuum and the FIR line overlap have been shown to be effective in several models, for example Gray, Field & Doel (1992), Pavlakis & Kylafis (1996). However, most of these models used the large velocity gradient (LVG) approximation, which makes it virtually impossible to study the region of parameter space where velocity shifts across the model are small compared to the local sound speed, and where thermal FIR line overlap only is present. As a large amount of velocity-driven FIR line overlap is a fundamental part of any LVG OH model, it is, in a way, unsurprising that such models find it essential.

To recover the detail of pumping schemes from a numerical model, a record of the algebraic operations which are performed on the system of equations must be stored. This allows coefficients of a partially-solved system to be decomposed into those of a less-processed form of the equations, building up a network of population flow cycles involved in pumping. The identification of such cycles was attempted by Sobolev (1986). These cycles are somewhat analogous to electrical circuits, obeying rules similar to Kirchoff's laws Sobolev & Deguchi (1994). A Monte-Carlo computer code based on this method has been applied to water masers Sobolev (1989) and to methanol masers Sobolev & Deguchi (1994). In both cases, the indications are that it may not be possible to identify simple pumping schemes in these molecules. The case of OH is discussed below. The tracing method is not Monte-Carlo, but computer-algebra based. The method is implemented in the computer code TRACER, and details appear in Gray, Howe & Lewis and Gray (2007).

2. Population tracing

2.1. *The parameter-space model*

The numerical solution used as the basis for population tracing is still drawn from a parameter-space search. However, the analysis, in terms of the pumping scheme, is completely different: instead of drawing an inference from the physical conditions supplied to a large number of models, a single zone from one model is examined in detail with TRACER. For the environments studied in the current work, the parameter-space models were all of the accelerated lambda-iteration (ALI) type, using LU-factorization as the numerical method. Local and non-local FIR line overlap were included.

2.2. *The* TRACER *model*

There are two parts to this model: one is written into a special subroutine of the ALI solver, which runs only once as an extra iteration when convergence has already been achived by the ALI method. In this final iteration, a naive method of solving the matrix is used for ease of human interpretation, and a log is maintained of the operations carried out on the matrix. In the naive method the all-process rate coefficient for the transition from level x to level y, with z eliminations to go, may be written

$$k^z_{x,y} = k^{z+1}_{x,y} + k^{z+1}_{x,z} k^{z+1}_{z,y} / k^{z+1}_{z,z} \tag{2.1}$$

The first term on the right represents the coefficient from the previous elimination, whilst the second term represents transfer between level x and level y via level z. The log of operations compares the size of these two terms and, according to the accuracy of the trace, determines whether both must be kept, or one can be omitted.

The operation log described above forms the input to the tracer code itself. This begins with an analytical expression for the inversion, derived from a small, highly processed, matrix with $z = 3$ or $z = 4$. Expressions for all four ground-state inversions appear in Section 3. Tracer algebraically expands the expression for a given inversion, considering antagonistic pairs of expressions that represent the forward and backward parts of each route. Every time an expression like the second term on the right-hand side of 2.1 must

https://doi.org/10.1017/S1743921307012501 Published online by Cambridge University Press

be included, a branch to a new route is introduced, leading to increased complexity. The trace is complete when all coefficients are the unprocessed originals that were fed into the matrix as input data. These have $z = N + 1$, where N is the number of energy levels in the model. There is no guarantee of underlying simplicity, and expressions could become completely unmanageable for values of z considerably smaller than $N + 1$.

3. Ground-state inversions

We present here the remaining ground-state inversions, as analytical solutions of either a 4×4 or 3×3 matrix. Obviously, the forms for the transitions which include level 4 are more complicated, but contain one layer of possible complexity fewer when TRACER is run. Values of $\mathcal{N}$ and X are given in Gray (2007).

It is convenient to break these expressions up into 'direct' and 'indirect' parts. The former involve no other uneliminated level, whilst the latter do: for example in the 1612-MHz inversion, 3.1, the 'direct' part involves only the maser levels, 2 and 3, whilst the indirect part also involves the other uneliminated level, level 1. Of course both the 'direct' and 'indirect' parts can involve, when expanded by TRACER, a large number of previously eliminated levels.

$$\Delta\rho_{32} = \frac{\mathcal{N}k^4_{1,2}}{D}\left\{(1+\eta)\left(\frac{k^4_{2,3}}{3} - \frac{k^4_{3,2}}{5}\right) + \frac{\eta k^4_{2,1}}{3} - \frac{k^4_{3,1}}{5}\right\} \tag{3.1}$$

$$\Delta\rho_{31} = \frac{\mathcal{N}k^4_{2,2}}{3D}\left\{k^4_{1,3} - k^4_{3,1} + \left(\frac{k^4_{1,2}k^4_{2,3} - k^4_{3,2}k^4_{2,1}}{k^4_{2,2}}\right)\right\} \tag{3.2}$$

$$\begin{aligned}\Delta\rho_{42} = \frac{\mathcal{N}'}{5}\Bigg\{&k^5_{2,4} - k^5_{4,2} + \frac{k^5_{1,1}}{X}\left(k^5_{2,3}k^5_{3,4} - k^5_{4,3}k^5_{3,2}\right) + \frac{k^5_{3,3}}{X}\left(k^5_{2,1}k^5_{1,4} - k^5_{4,1}k^5_{1,2}\right)\\ &+ \frac{k^5_{2,1}k^5_{1,3}k^5_{3,4} - k^5_{4,3}k^5_{3,1}k^5_{1,2}}{X} + \frac{k^5_{2,3}k^5_{3,1}k^5_{1,4} - k^5_{4,1}k^5_{1,3}k^5_{3,2}}{X}\Bigg\}\end{aligned} \tag{3.3}$$

$$\begin{aligned}\Delta\rho_{41} = \mathcal{N}'\Bigg\{&\frac{k^5_{1,4}}{5} - \frac{k^5_{4,1}}{3} + \frac{k^5_{3,3}}{X}\left(\frac{k^5_{1,2}k^5_{2,4}}{5} - \frac{k^5_{4,2}k^5_{2,1}}{3}\right) + \frac{k^5_{2,2}}{X}\left(\frac{k^5_{1,3}k^5_{3,4}}{5} - \frac{k^5_{4,3}k^5_{3,1}}{3}\right)\\ &+ \frac{k^5_{1,2}k^5_{2,3}k^5_{3,4}}{5X} - \frac{k^5_{4,3}k^5_{3,2}k^5_{2,1}}{3X} + \frac{k^5_{1,3}k^5_{3,2}k^5_{2,4}}{5X} - \frac{k^5_{4,2}k^5_{2,3}k^5_{3,1}}{3X}\Bigg\}\end{aligned} \tag{3.4}$$

4. Example pump traces

4.1. *1612 MHz in a detached Mira envelope*

This study considered the behaviour of masers in the envelope of an AGB star at the end of a phase of rapid mass loss: as it finishes, the envelope detaches from the star, leaving a hollow shell. The pumping scheme at shell detachment was compared with the scheme 40 yr later, when the maser emission at 1612 MHz had become very weak. Further details appear in Gray, Howe & Lewis (2005).

https://doi.org/10.1017/S1743921307012501 Published online by Cambridge University Press

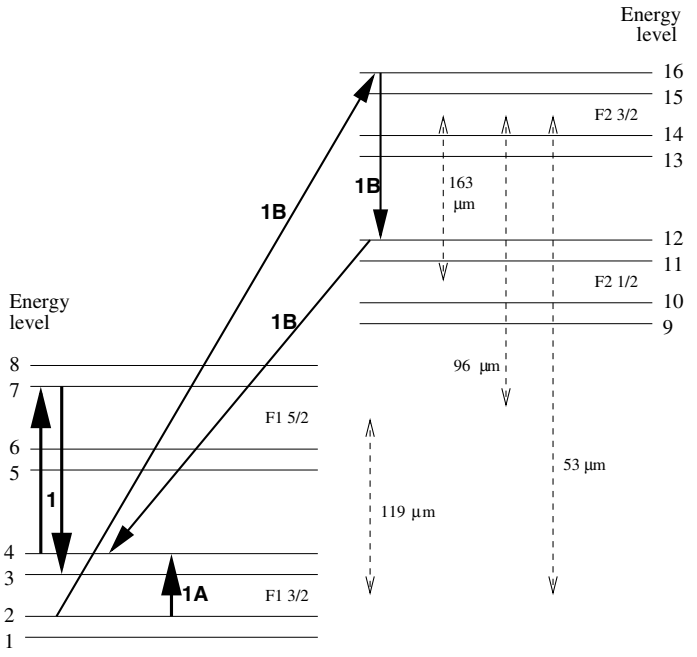

Figure 1. The 'direct' part of the 1612-MHz pump at shell detachment. OH levels are numbered by increasing energy. Rotational, lambda-doubling and hyperfine splittings are shown, but not to scale. Approximate rotational transition wavelengths are marked in μm. Transitions shared by more than one route are shown only once. Reverse transitions are omitted.

We traced the 'direct' part of the pump, a positive-definite multiplier times $k_{2,3}^4/3 - k_{3,2}^4/5$, and the 'indirect' part, which can be written as a multiplier times the expression,

$$\frac{1}{k_{1,2}^4}\left[\left(\frac{k_{2,1}^4}{3}\right)k_{1,3}^4 - k_{3,1}^4\left(\frac{k_{1,2}^4}{5}\right)\right].$$

At shell detachment, the 'direct' part supplied approximately 2/3 of the inversion. The most significant change over 40 yr was the complete loss of the 'indirect' routes, which by that time contributed significant absorption. The 'direct' and 'indirect' parts of the pump are shown respectively in figure 1 and figure 2. The notation used for the routes employs numbers for the primary branches, capital letters for secondary branches, and roman numerals for tertiary branches. As expected, the most important radiative pump employs 53 μm radiation, but the 'indirect' routes are the more dependent. Therefore, as the hollow shell expands and cools the energy density of the 53 μm radiation falls, leading to preferential collapse in the part of the pump which operates via level 1 (the 'indirect' part).

4.2. *1612 and 1667 MHz in a supergiant envelope*

The pumping schemes for OH masers in a larger, warmer envelope were traced. The parameters of the envelope were loosely based on the red supergiant, S Perseii (spectral type M4.5). The most important routes (solid lines) are displayed in figure 3 for the 1665-MHz main line. The 1612-MHz pump has much in common with figure 3, and both are based on initial absorption of 35 μm radiation. In the 1612-MHz pump, the most important route is completed by the expected decay to the rotational ground state Elitzur, Goldreich & Scoville (1976), but for 1665 MHz, we see from figure 3 that the

https://doi.org/10.1017/S1743921307012501 Published online by Cambridge University Press

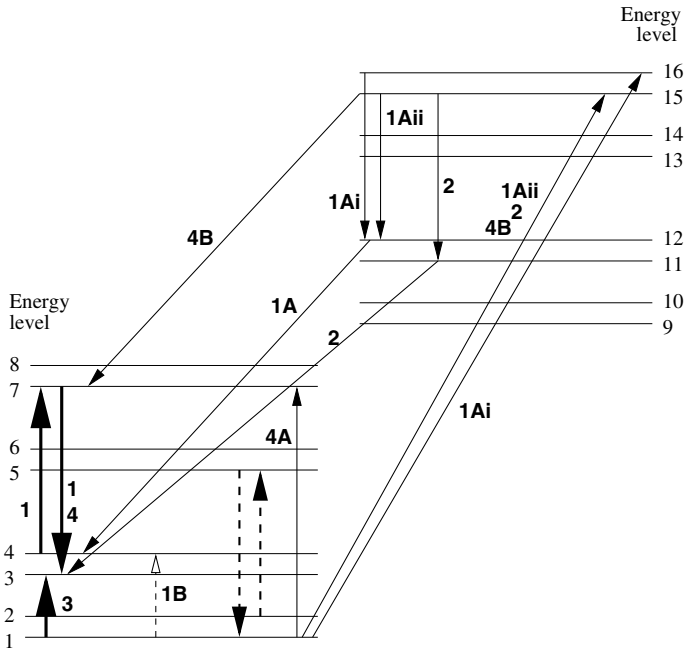

Figure 2. As figure 1, but for the 'indirect' part of the pump, which operates via level 1.

radiative cascade does not complete, and three additional absorptions result in transfer to the $^2\Pi_{3/2}$ ladder, followed by radiative decays through that stack of levels to the upper level of the maser.

4.3. *Main lines in a star-forming region*

The ALI solution was drawn from a region of a parameter space search with very high main-line ground-state inversions, yielding unsaturated integrated gains of 20.039 at 1665 MHz and 35.661 at 1667 MHz. The ALI slab had no velocity shift or microturbulence and constant physical conditions: $n_{H_2} = 10^7\,\mathrm{cm}^{-3}$; [OH] = 0.2 ppm; $\mathrm{T}_K = 30\,\mathrm{K}$ and $\mathrm{T}_d = 70\,\mathrm{K}$. Eighty logarithmically-spaced model slabs covered a depth of 2×10^{13} m.

The trace of the 1665-MHz pump appears in figure 4, showing the five most important routes, contributing 82% of the total inversion. These were expanded from both the 'direct' and 'indirect' parts of the pump. As pump rates, the five routes contribute, (i) $(\mathrm{k}^6_{1,5}\mathrm{k}^6_{5,3} - \mathrm{k}^6_{3,5}\mathrm{k}^6_{5,1})\ /\mathrm{k}^6_{5,5} = 6.01\times\ 10^{-5}\,\mathrm{s}^{-1}$; (ii) $(\mathrm{k}^6_{1,5}\mathrm{k}^6_{5,2}\mathrm{k}^6_{2,4}\mathrm{k}^6_{4,3} - \mathrm{k}^6_{3,4}\mathrm{k}^6_{4,2}\mathrm{k}^6_{2,5}\mathrm{k}^6_{5,1})/(\mathrm{k}^4_{2,2}\mathrm{k}^5_{4,4}\mathrm{k}^6_{5,5}) = 4.86\times\ 10^{-5}\,\mathrm{s}^{-1}$; (iii) $(\mathrm{k}^5_{1,4}\mathrm{k}^5_{4,3} - \mathrm{k}^5_{3,4}\mathrm{k}^5_{4,1})\ /\mathrm{k}^5_{4,4} = 2.72\times\ 10^{-5}\,\mathrm{s}^{-1}$ and two more minor terms totalling $2.46\times\ 10^{-5}\,\mathrm{s}^{-1}$. Route (i) is especially simple, having no additional complexity on expansion back to original coefficients. 73% of route (ii) is formed from three sub-routes, A (via levels 4, 6 and 7), B (via level 20) and C (via levels 10 and 14). Route (iii) is even more complex with only 50% of its strength coming from the most important three subroutes: A (via levels 9, 10, 14 and 20), B (via levels 10 and 14) and C (direct collisional transfer from level 4 to level 3).

The traced pump routes for 1667 MHz are shown in figure 5. Both main-line pump routes lie predominantly in the $^2\Pi_{3/2}$ ladder. Most transitions are radiative, but there are several important collisional links. The strongest route, route (i), in both main lines is very similar, with a radiative upward pump, and a collisional decay (see the bold, solid routes in figure 4 and figure 5. The route is $1 \rightarrow 5$, $5 \rightarrow 3$ for 1665 MHz, and one level higher at 1667 MHz. Further details appear in Gray (2007).

https://doi.org/10.1017/S1743921307012501 Published online by Cambridge University Press

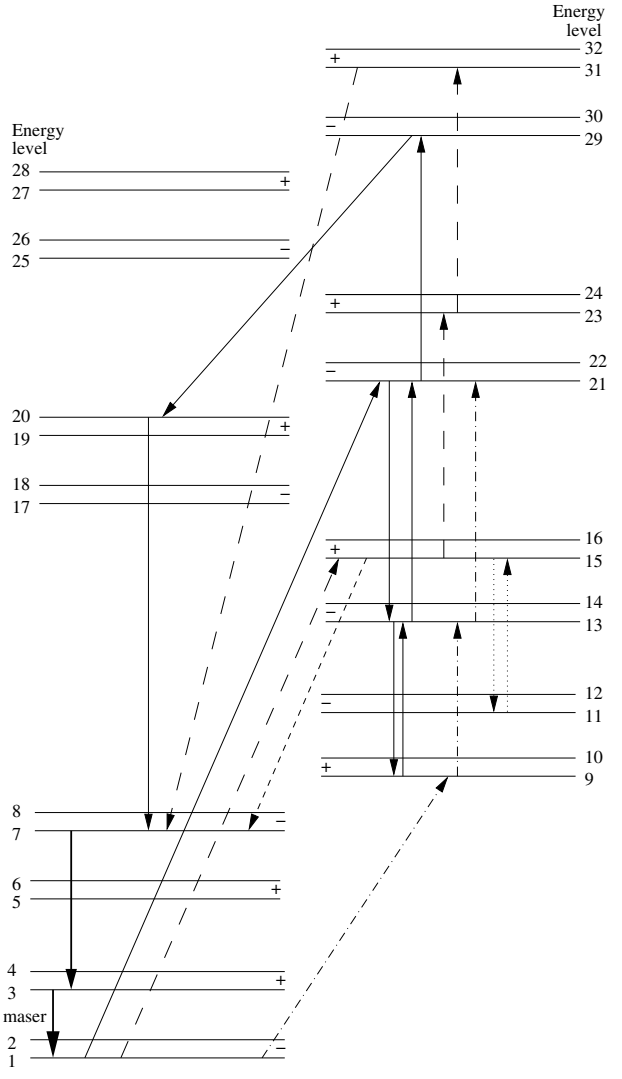

Figure 3. Pump routes for 1665 MHz in an M-supergiant. The most important routes are shown as solid lines, followed in order of inverting effect by those shown in the long dashed, chained, short-dashed and dotted styles.

A more detailed analysis of the strongest routes only, breaking the coefficients down into their individual processes, shows a hierarchy of processes with the Einstein A-values dominating over the radiative pumps of type BJ, and these in turn dominating over the collisions. Values in Hz for the 1665-MHz line are: $C_{5,3} = 3.75(-4); C_{3,5} = 1.13(-5)$ $A_{5,1} = 0.1244; B_{5,1}\bar{J}_{1,5} = 2.160(-2); C_{5,1} = 3.16(-4)$ $B_{1,5}\bar{J}_{1,5} = 3.60(-2); C_{1,5} = 9.48(-5)$. Ignoring products of collisional terms, and $C_{3,5}$ in comparison to $C_{5,3}$, we find the route (i) expression is $k_{1,5}k_{5,3} - k_{3,5}k_{5,1} \sim B_{1,5}\bar{J}_{1,5}C_{5,3} - A_{5,1}C_{3,5}$. In terms of downward coefficients only, and as $h\nu/(kT_k) \gg 1$ for the $5 \rightarrow 1$ transition, this reduces to $k_{1,5}k_{5,3} - k_{3,5}k_{5,1} \sim K((\bar{J}_{1,5}/B_\nu(T_K) - 1)$ where K is a positive definite expression which cannot decide the sign of the inversion. Therefore, the inversion depends on two things: firstly the rotational energy gap is large compared with T_K, favouring $C_{5,3}$ over $C_{3,5}$; secondly, the dust continuum, at $T_d = 70\,\mathrm{K}$, is hotter than the kinetic temperature, allowing mean intensity greater than a black-body at T_K. An

https://doi.org/10.1017/S1743921307012501 Published online by Cambridge University Press

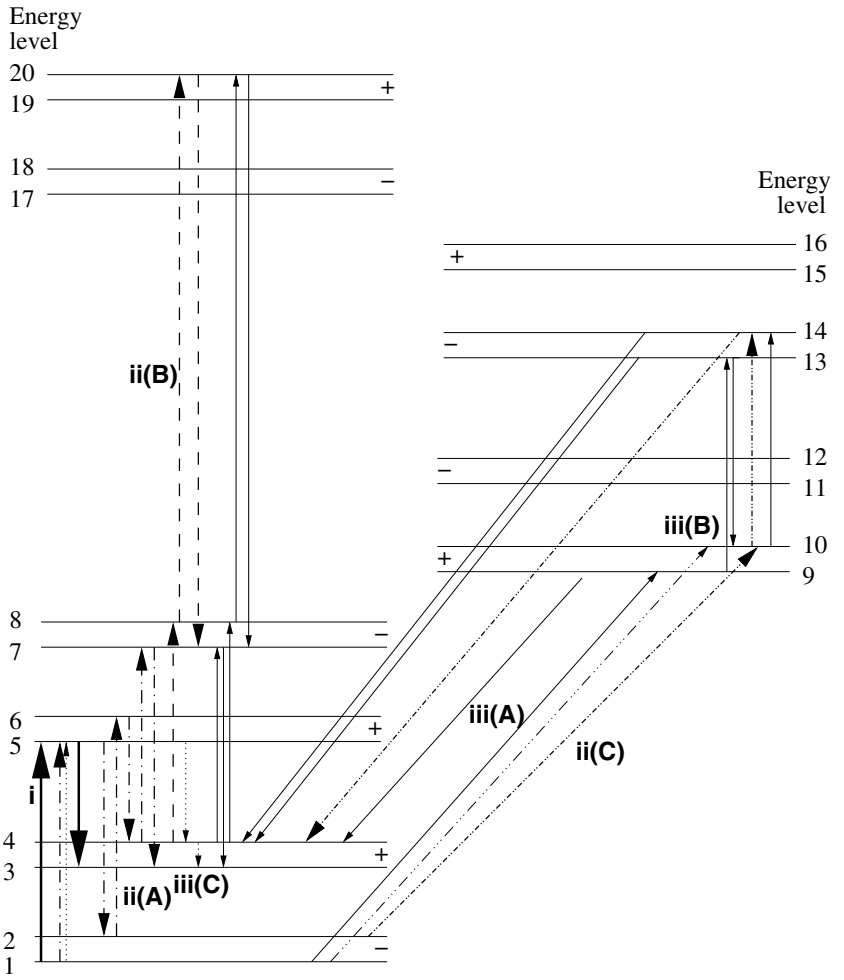

Figure 4. Strongest pump routes at 1665 MHz: transitions appearing in more than one route are repeated, but reverse routes are not shown for clarity.

analysis of the ALI slabs near the inner boundary in terms of radiation diffusion shows that the source of the dust radiation is the optically thick boundary itself. Radiation in the pumping 5, 1 pumping line penetrates because it is effectively scattered and not thermalised.

Mirror routes, an example being the a transfer from level 3 to level 5 via level 7 (instead of 5) in the 1665-MHz case, do not cancel the inverting effect of the pump because of parity propensity in the collisions of OH with para-H_2. This propensity makes $C_{7,1}$ significantly smaller than $C_{5,3}$ at values of T_K below 100 K, where the para-species of H_2 dominates.

5. Conclusions

It is possible to obtain detailed pumping routes generating the great majority of the inversion from a small fraction of the input coefficients. AGB and supergiant traces broadly support earlier theory. Significant contributions to main-line pumps have just two steps: radiative 'up' and collisional 'down'.

https://doi.org/10.1017/S1743921307012501 Published online by Cambridge University Press

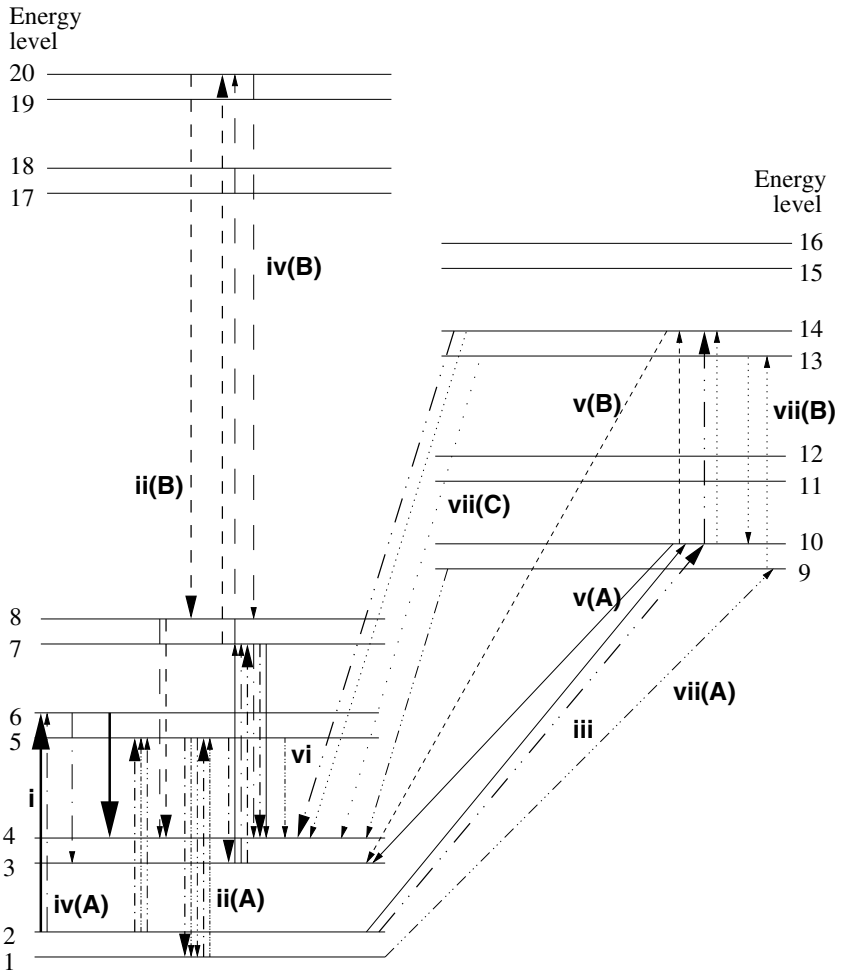

Figure 5. As figure 4 but for 1667 MHz. The seven routes shown have relative strengths 1.0, 0.413, 0.290, 0.225, 0.228, 0.203, 0.112, with route i being the strongest.

References

Bujarrabal, V., Guibert, J., & Nguyen-Q-Rieu 1980, *A&A* 84, 311
Dickinson, D. F. 1987, *ApJ* 313, 408
Elitzur, M. 1976, *ApJ* 203, 124
Elitzur, M. 1981, in: I. Iben & A. Renzini (eds.), *Physical Processes in Red Giants*, (Dordrecht: Reidel), p. 363
Elitzur, M., Goldreich, P., & Scoville, N. 1976, *ApJ* 205, 384
Gray, M. D. 2007, *MNRAS* 375, 477
Gray, M. D., Field, D., & Doel, R. C. 1992, *A&A* 262, 555
Gray, M. D., Howe, D. A., & Lewis, B. M. 2005, *MNRAS* 364, 783
He, J. H., & Chen, P. S. 2004, *New Astronomy* 9, 54
He, J. H., Szczerba, R., Chen, P. S., & Sobolev, A. M. 2005, *A&A* 434, 201
Pavlakis, K. G., & Kylafis, N. D. 1996, *ApJ* 467, 309
Sobolev, A. M. 1986, *Sov. Ast.* 30, 399
Sobolev, A. M. 1989, *Astronomiche Nachrichten* 310, 343
Sobolev, A. M., & Deguchi, S. 1994, *ApJ* 433, 719

https://doi.org/10.1017/S1743921307012501 Published online by Cambridge University Press